J Mater Sci: Mater Electron (2015) 26:3206–3214
DOI 10.1007/s10854-015-2818-5

# Study on growth mechanism and optical properties of ZnSe nanoparticles

**Bo Feng · Jian Cao · Donglai Han · Shuo Yang · Jinghai Yang**

Received: 19 December 2014 / Accepted: 6 February 2015 / Published online: 13 February 2015


**Abstract** ZnSe nanoparticles with the cubic zinc blende structure were synthesized by a triethanolamine (TEA)-assisted solvothermal method without surfactants and templates. The effects of the TEA on the growth mechanism of ZnSe nanoparticles were analyzed. Photoluminescence measurements showed that the intensity of the defect-related emission band varied with the volume of TEA, as different types of defects were dominant in the ZnSe nanoparticles. Moreover, the emission band centered at 545 nm was attributed to the recombination of a donor–acceptor pair involving Zn vacancies, while the emission band centered at 668 nm was due to the stacking faults, twinning defects and some point defects. In Raman spectra, a clear shift of the transverse and longitudinal optical phonon modes, as well as a broadening of the longitudinal optical phonon peak were observed for ZnSe nanoparticles.

## 1 Introduction

Inorganic semiconductor nanocrystals have been studied extensively from experimental and theoretical viewpoints, owing to their potential applications in solar energy conversion, photocatalysis, and other applications in the optoelectronic industry [1–5]. Nanomaterials of different II–VI semiconductors have also attracted much attention due to their promising characteristics for electronic, optical, photonic and catalytic applications [6–8]. Wide band-gap Zn based semiconducting materials are very efficient emitters in the blue–green spectral region and consequently their yield is expected to be greater than that of usual III–V devices [9, 10]. In the past decades, the majority of research on II–VI semiconductors has focused on ZnO, ZnS, CdSe, and CdS, with a very limited number of reports on ZnSe nanostructures. For example, ZnO nanostructures are considered to be one of the most investigated materials for different nanotechnological applications [11–14]. Gedamu et al. [15] reported that ZnO nanostructure-based UV photodetectors had been synthesized by a rapid fabrication technique, making such ZnO nanotetrapods potential candidates for various nanosensor applications. Recently, the wide-band-gap II–VI semiconductor material, zinc selenide, has been studied extensively due to wide-ranging applications in the fields of light-emitting devices, short-wavelength lasers, blue laser diodes, solar cells, sensors, and optical recording materials [16, 17]. In particular, ZnSe has a direct band gap of 2.67 eV and a large exciton binding energy of 21 meV at room temperature [18–20]. Moreover, ZnSe is of strong interest as a potential material for fabricating short-wavelength devices, as ZnSe nanomaterials exhibit a tunable blue-ultraviolet (UV) luminescence [21, 22]. For cadmium-based systems such as CdSe, this UV range is practically unobtainable, this in addition to the toxicity of cadmium, reiterates the desire to synthesize high quality ZnSe nanocrystals [23].

Various methods have been used to synthesize ZnSe nanoparticles with controlled morphology and structure

B. Feng (✉) · J. Cao · J. Yang (✉)
Key Laboratory of Functional Materials Physics and Chemistry of the Ministry of Education, Jilin Normal University, Haifeng Street No. 1301, Siping 136000, People's Republic of China
e-mail: fengbosiping@126.com

J. Yang
e-mail: jhyang1@jlnu.edu.cn

D. Han · S. Yang
Key Laboratory of Excited State Physics, Changchun Institute of Optics, Fine Mechanics and Physics, Chinese Academy of Sciences, 3888 Eastern Nan-Hu Road, Changchun 130033, People's Republic of China

[24–26]. For example, Quinlan et al. [27] utilized the reverse micelle technique using an ion exchange reaction that produced cubic ZnSe nanoparticles. Zhu et al. [28] reported that ZnSe nanoparticles of about 3 nm in size had been prepared by sonochemical irradiation of an aqueous selenourea and zinc acetate solution under argon. The sonochemical method has been used extensively to generate novel materials with unusual properties, as the method allows the formation of particles of a much smaller size and higher surface area. However, most of these methods involve the use of sophisticated equipment with toxic and sometimes explosive starting materials, which are not environmentally benign [29]. Xiong et al. [30] reported synthesis of spherical ZnSe nanoparticles of cubic structure. However, the reaction required a longer time and the selenium precursor used was unstable at room temperature. In order to attain an environmentally friendly technology, it is necessary to use greener methods to synthesize ZnSe nanomaterials in mild reaction conditions. Solvothermal synthesis has become a facile and promising approach to solve the above problems. The chemicals used in solvothermal synthesis are commercial standards, relatively inexpensive and the reaction can be completed under relatively moderate conditions. The solvothermal synthesis approach is considered as an effective and economical route for large scale production. Moreover, several groups have synthesized ZnSe nanostructures by the addition of triethanolamine (TEA) in aqueous solution. TEA has gained interest in metal coordination chemistry and has been proven to be beneficial in controlling particle growth [31]. Moreover, the size of the ZnSe nanoparticles can be controlled by using different amounts of TEA. The exact mechanism of the origin and variation in PL emission properties is still unclear, due to the complexity of the photochemistry in inorganic semiconductor nanocrystals. For ZnSe nanoparticles with large surface to volume ratios, PL properties are generally related to their surface structure [32]. The intensity of PL signals typically receives most of the attention in the analysis of interfaces. This is due to its dependence on the rate of radiative and non-radiative events, which in turn depend on the density of non-radiative interface states [33]. Dynamic growth processes play an important role in defining the surface structure of ZnSe nanoparticles and hence the PL properties.

In this paper, we synthesize the cubic ZnSe nanoparticles with different particle size, by only changing the amount of TEA. The growth mechanism of the ZnSe nanoparticles is investigated. TEA has been proven to be beneficial in controlling the particle growth. The solvothermal method is advantageous, as it can be executed within a short period of time and under ambient environmental conditions, making it efficient and economical. The optical properties of the ZnSe nanoparticles obtained by using different amounts of TEA are discussed in detail. Analysis of the deep defect-related emission is done for ZnSe nanoparticles obtained by using different amounts of TEA.

## 2 Experimental section

### 2.1 Preparation

All chemicals were of analytical grade and used as received without further purification.

The synthesis of ZnSe precursor was carried out by the following procedures: $Zn(NO_3)_2{\cdot}6H_2O$ (0.5 mmol) was dissolved in NaOH to form a transparent solution, after which anhydrous TEA was added to the solution and stirred for 30 min, before the addition of selenium powder (99.95 %) (0.5 mmol). Then, the mixed solution was transferred into an 80-ml stainless steel Teflon-lined autoclave, which was filled to 75 % of its capacity. A range of mixed solvents composed of TEA at the volumes of 40 and 50 ml and deionized water were produced. The autoclaves were heated to 180 °C for 24 h and then cooled to room temperature. Products were then washed with distilled water and absolute alcohol three times before being dried in a vacuum at 60 °C for 1 h. To obtain the ZnSe nanoparticles, the products were calcined in a tube furnace under an argon atmosphere.

### 2.2 Characterization

The crystal structure and phase of the synthesized products were characterized by a MAC Science MXP-18 X-ray diffractometer (XRD) (with 40 kV and 200 mA, Cu Ka radiation with $\lambda = 1.5406$ Å). Transmission electron micrograph (TEM) was taken with a JEM-2100 transmission electron microscope at an accelerating voltage of 200 kV. The specimen was prepared by depositing a drop of the dilute sample solution in 2-propanol on a carbon-coated copper grid and drying at room temperature. The PL measurement was carried out at room temperature, using 325 nm as the excitation wavelength, and a He–Cd laser as the excitation source. The Raman scattering studies were performed with a 1000B Renishaw micro-Raman system in the back-scattering configuration, and the excitation source was the 514.5 nm line of an Ar + laser for which ZnSe was transparent. The beam was focused through a microscope objective on the samples as a 1 μm circular spot.

## 3 Results and discussion

X-ray diffraction is widely used as a conventional and routine technique to determine the crystal structure of

powder samples. The X-ray diffraction patterns of the prepared ZnSe samples with different concentrations of TEA are shown in Fig. 1. For the samples obtained by using 40 ml of TEA as shown in Fig. 1a, the characteristic diffraction peaks centered at 27.22°, 45.18°, 53.54°, 65.82° and 72.62° closely match the typical (111), (220), (311), (400) and (331) crystal planes of the cubic zinc blende ZnSe ($F\bar{4}3m$, JCPDS file #37-1463). For the samples obtained by using 50 ml TEA as shown in Fig. 1b, the peaks centered at 27.18°, 45.16°, 53.52°, 65.82° and 72.58° also match the corresponding diffraction planes of the cubic zinc blende ZnSe. The intensities of the peaks in Fig. 1a is stronger than that of the peaks in Fig. 1b, which indicates that the samples obtained by using 40 ml of TEA have better crystallinity. Moreover, the lattice constant 'a' for the cubic structure can be determined from the relationships:

$$\text{Cubic}: 1/d_{hkl}^2 = \left(h^2 + k^2 + l^2\right)/a^2$$

The average lattice constant of 'a' for ZnSe nanoparticles obtained by using 40 and 50 ml of TEA is found to be 5.671 and 5.673 Å, respectively. Both are slightly larger than the standard value of 5.668 Å. These results indicate that the ZnSe nanoparticles are under tensile strain. No other diffraction peaks can be found in the pattern, indicating no impurity is present in the as-synthesized samples. The formation of the zinc-blende rather than the wurtzite phase ZnSe originates from the fact that the formation of this phase is more thermodynamically favorable at low temperatures [34, 35].

Figures 2 and 3 show the TEM images of the ZnSe samples obtained by using different volumes of TEA. Uniform small nanoparticles (average size about 20 nm) are yielded when 40 ml of TEA is introduced into the system as shown in Fig. 2a. Figure 2b, c are the high resolution transmission electron microscope (HRTEM) of the ZnSe nanoparticles obtained by using 40 ml of TEA, which exhibits some point defects and some structural defects in the form of stacking faults. And the point defects are obvious and dominant. Figure 2d displays the corresponding SAED pattern for ZnSe nanoparticles obtained by using 40 ml of TEA. This figure shows a set of sharp spots that clearly reveal the single crystalline nature and cubic phase of the ZnSe nanoparticles, as confirmed by the behaviour of the lattice fringes.

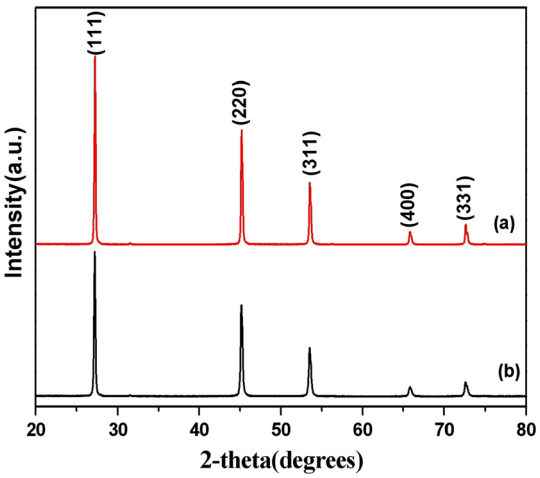


**Fig. 1** XRD patterns of ZnSe nanoparticles synthesized using TEA, *a* 40 ml and *b* 50 ml

Figure 3a shows the typical TEM morphologies of the ZnSe samples obtained in the solvothermal system with 50 ml of TEA. The TEM image indicates that the nanoparticles are well dispersed and spherical in shape. The average particle size is approximately 10 nm. The particle size decreases with the volumes of TEA increasing. Figure 3b, c are the high resolution transmission electron microscope (HRTEM) of the ZnSe nanoparticles obtained by using 50 ml of TEA, which exhibits a high density of stacking faults, twinning defects and some point defects. Most defects are in the form of stacking faults. The crystalline nature of the ZnSe nanoparticles obtained by using 50 ml of TEA is confirmed by their electron diffraction patterns, as presented in Fig. 3d. These diffraction rings can be identified as those from the zinc-blende phase of ZnSe, which is consistent with the results from the XRD pattern. Nanomaterials have, in general large surface to volume ratio. Hence, large numbers of defects are inherently present in nanocrystalline materials. These defects may include dislocations, vacancies, interstitials and substitutionals.

Different size of ZnSe nanoparticles can be achieved by using different amounts of TEA. During the entire process, TEA plays an important dual role, which not only serves as a complexing reagent to influence the size of the ZnSe nanoparticles but also releases $OH^-$ ions to change the alkaline environment [36]. In the TEA-assisted hydrothermal process, TEA, being a cationic surfactant, interacts with $[Zn(OH)_4]^{2-}$ to form TEA ligands, due to Coulomb force action. The formed TEA ligands have the ability to selectively adsorb onto specific crystal planes and restrain the anisotropic growth of ZnSe crystallites, thereby driving the ZnSe nuclei to form sufficiently stable and uniform nanoparticles in the solution. When 40 ml of TEA is used in the reaction, the ZnSe nanoparticles become irregular in shape and relatively large in size, typically around 20 nm. This is most likely due to there being insufficient TEA to stabilize the nanocrystals as they grow. When 50 ml of TEA is used, the nanoparticles are almost spherical, with an average size of 10 nm. In this case, it is likely that the competing reaction is more dominant with

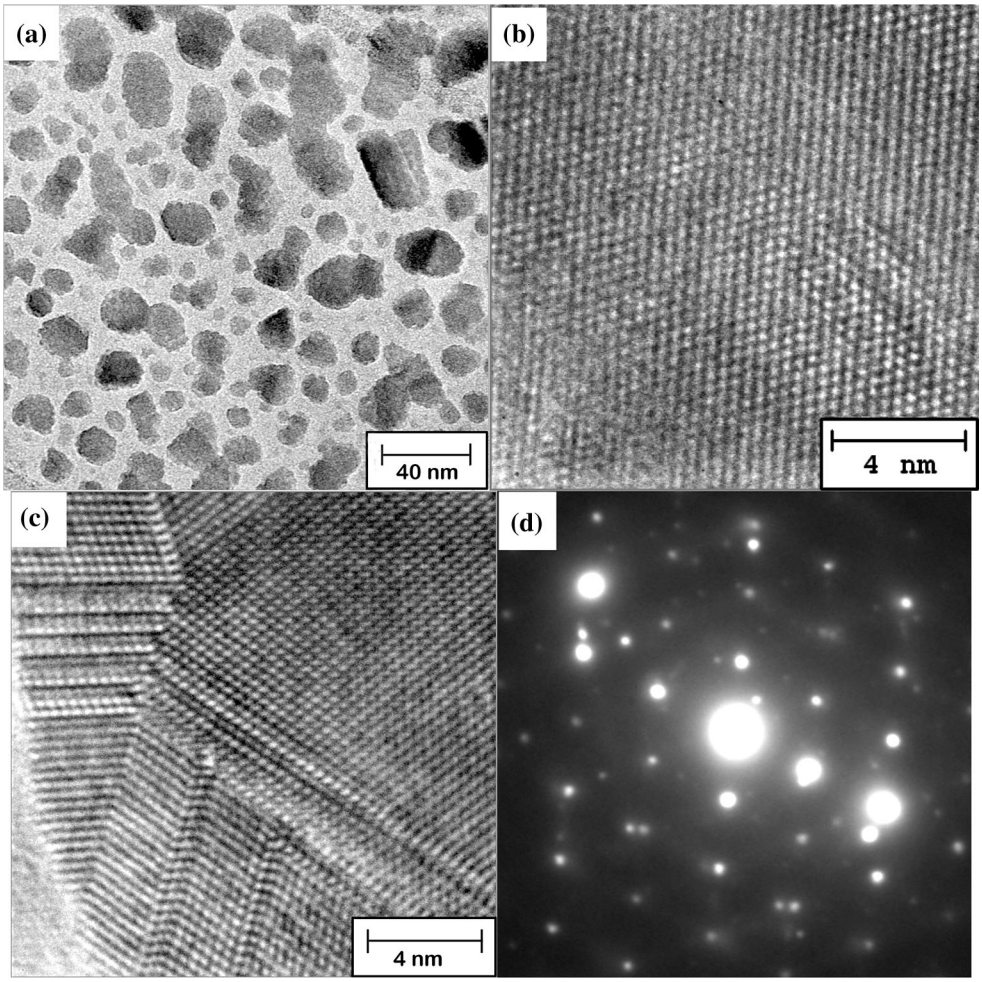


**Fig. 2** TEM image (**a**), high-resolution TEM image (**b**) and (**c**), SAED patterns (**d**) of ZnSe nanoparticles obtained by using 40 ml of TEA

the higher TEA concentrations. The reaction process can be mainly expressed as follows:

$$Zn^{2+} + 2OH^- \rightarrow Zn(OH)_2$$

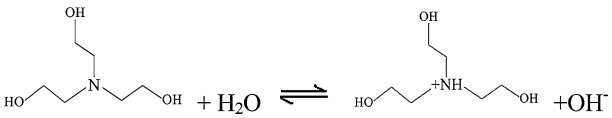


$$Zn(OH)_2 + 2OH^- + TEA \rightarrow \left[Zn(OH)_4\right]^{2-} - TEA$$

$$Zn^{2+} + nTEA \rightleftharpoons \left[Zn(TEA)_n\right]^{2+}$$

$$\left[Zn(TEA)_n\right]^{2+} + Se^{2-} \rightarrow ZnSe + nTEA$$

A schematic illustration of the growth procedures of ZnSe nanoparticles obtained by using 40 and 50 ml of TEA is shown in Fig. 4. The $[Zn(TEA)_n]^{2+}$ complex is increasingly stable with higher amounts of TEA. Therefore, when the Se source is added, only a small amount of ZnSe will nucleate, and grow gradually over time as $Zn^{2+}$ is released from the complex. Accordingly, point defects and structural defects are observed in the ZnSe nanoparticles when using different volumes of TEA. The larger the quantity of TEA, the slower the releasing rate of $Zn^{2+}$. Consequently, the more structural defects are present in the obtained ZnSe nanoparticles. In addition, there are more Zn vacancies in the ZnSe nanoparticles when 40 ml of TEA is used, while there are more structural defects in the ZnSe nanoparticles when 50 ml of TEA is used.

To investigate their optical properties, the room-temperature photoluminescence spectra of the as-prepared ZnSe samples obtained by using different volumes of TEA are recorded and compared in Fig. 5. Figure 5a shows the PL spectrum for ZnSe nanoparticles obtained by using 40 ml of TEA. The spectrum exhibits a weak blue emission band centered at 448 nm, a much wider and stronger emission band from 470 to 630 nm which is centered at 545 nm, and a very weak emission peak centered at 674 nm. The emission band at 448 nm is usually attributed

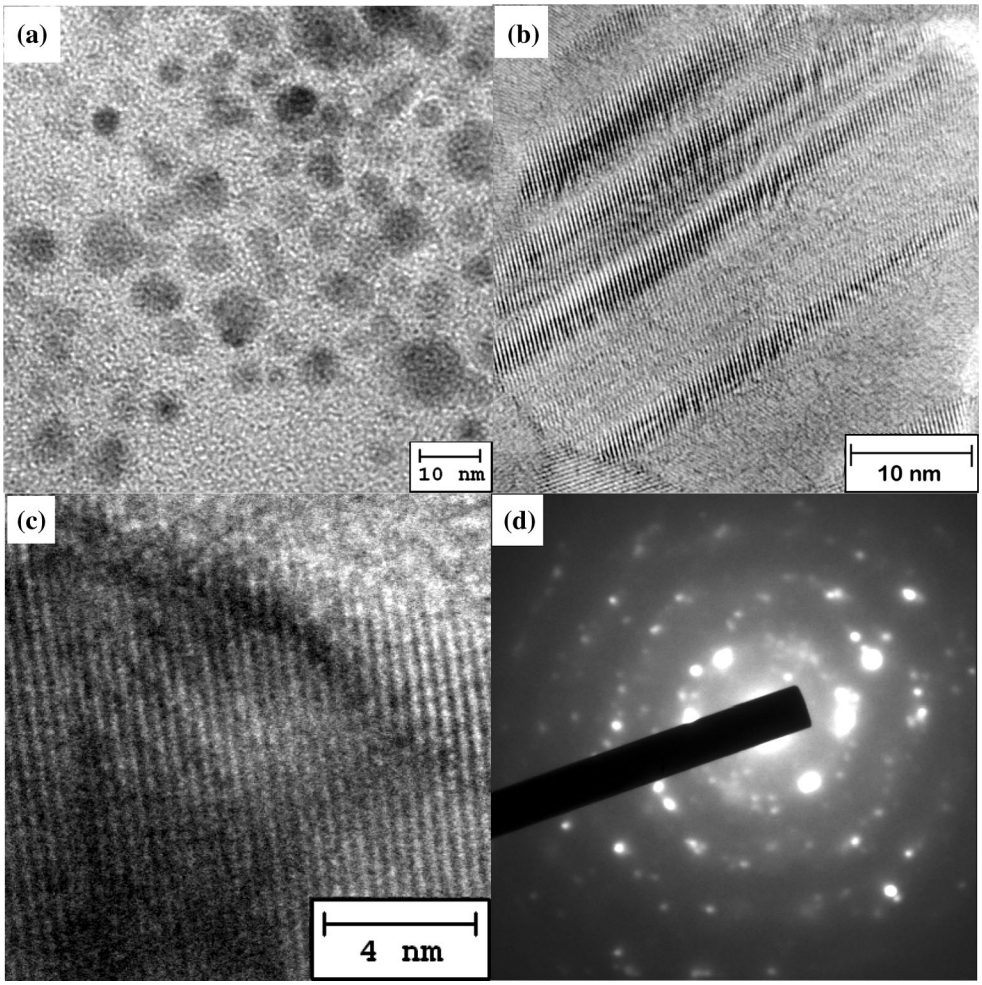


**Fig. 3** TEM image (**a**), high-resolution TEM image (**b**) and (**c**), SAED patterns (**d**) of ZnSe nanoparticles obtained by using 50 ml of TEA

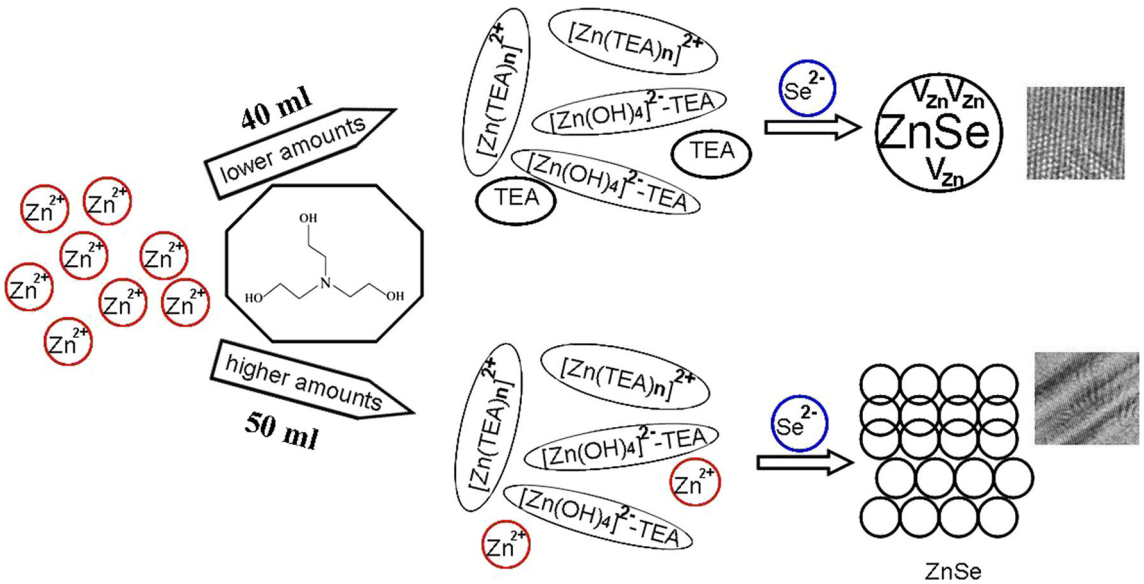


**Fig. 4** A schematic illustration of the growth procedures of ZnSe nanoparticles obtained by using different quantities of TEA

to the near-band edge (NBE) emission for ZnSe [37], while the emission band from 470 to 630 nm and the very weak emission peak centered at 674 nm represent the defect-related emission [38]. As the diameters of ZnSe nanoparticles are significantly larger than the exciton Bohr diameter, the band gaps are similar to that of the bulk ZnSe materials. Geng et al. [39] reported that the ZnSe nanoparticles showed a weak blue emission band at approximately 450 nm and a strong orange emission band at about 560 nm. These results are relatively consistent with our findings. In fact, the PL of ZnSe crystals is usually reported to be centered at 442 nm for the band gap emissions and 500–560 nm for the doped ion emissions [38]. Therefore, we conclude that the strong emission from the prepared ZnSe nanoparticles demonstrates the influence of the Zn-vacancies. For the defect-related emission band in PL spectra in Fig. 6, the black line denotes the experimental data (part of curve (a) in Fig. 5), the red circles represent the fitting curves, and the deconvoluted individual peaks are depicted by green lines. The PL spectrum in Fig. 6 shows a broad emission band that can be decomposed into four peaks. These can be attributed to the following origins: 502 nm to Zn vacancies [40], 545 nm to Zn vacancies and interstitials [41], 590 nm to lattice defects [41], 672 nm to stacking faults [42]. Previously, Panda et al. reported that the PL spectrum of ZnSe nanowires emits at approximately 500 and 546 nm at room-temperature. As well as the nature of the rods, this emission is associated with the vacancies of Zn in ZnSe [40]. Wei et al. reported that the emission at 550 nm of ZnSe hollow microspheres is related to deep-defects, which are attributed to the recombination of a donor–acceptor pair involving Zn vacancies and interstitials as well as surface emission. The weak yellow–orange emission at 600 nm are associated with the Zn/Se vacancies and interstitial sites of

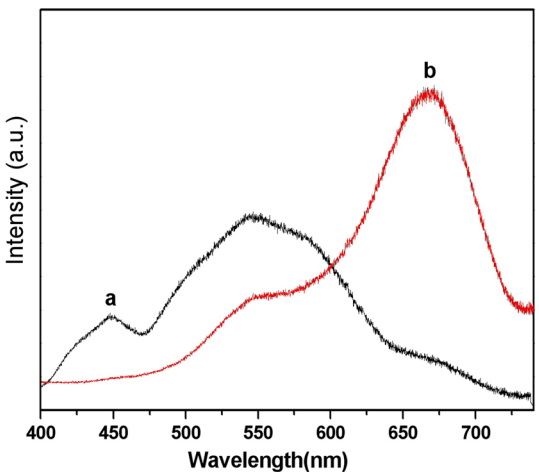


**Fig. 5** Room-temperature PL spectrum (excited at 325 nm) of ZnSe nanoparticles synthesized using TEA, *a* 40 ml and *b* 50 ml

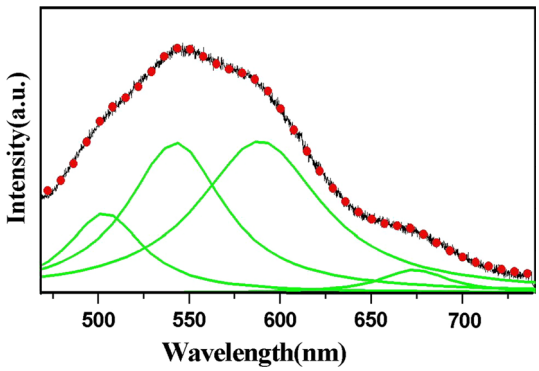


**Fig. 6** Defect-related emission band in PL spectrum of ZnSe nanoparticles synthesized using 40 ml of TEA where four components (*green curves*) are used to deconvolute the experimental peak (Color figure online)

ZnSe, or lattice defects, such as dislocations, stacking faults and nonstoichiometric defects [41]. The difference between these and our results is most likely due to the difference in crystal structure between bulk ZnSe crystals and the synthesized nanoparticles.

In contrast, the PL spectrum for ZnSe nanoparticles obtained by using 50 ml TEA, as shown in Fig. 5b, exhibits two defect-related emission bands, one of which is centered at 545 nm and the other centered at 668 nm, none of which appear at the near-band edge emission peak [43, 44]. It is noted that the NBE emissions of ZnSe nanoparticles do not exist. Xiang et al. [45] found that the photoluminescence of ZnSe samples demonstrated a strong green emission from room temperature down to 10 K. Moreover, Pol et al. [42] reported that ZnSe nanoparticles showed a broad red emission band extending from 550 to 760 nm. In these reports, there is no NBE emission of ZnSe nanomaterials, which is consistent with our results.

Three main changes are observed in the emission intensity for the prepared ZnSe nanoparticles when the TEA volumes increase from 40 to 50 ml. First, the peak at 448 nm, attributed to the near-band edge emission of ZnSe, disappears. Second, the intensity of the peak centered at 545 nm becomes weaker. Third, the intensity of the peak centered at 668 nm becomes stronger.

The defect-related emission is often attributed to stacking faults, twinning defects and nonstoichiometric defects, such as intrinsic point defects (vacancies and interstitials). The defect-related emission centered at 545 nm is attributed to recombination of a donor–acceptor pair involving Zn vacancies [40], while the emission centered at 668 nm is ascribed to stacking faults, twinning defects and some point defects [42]. For ZnSe nanoparticles obtained by using 40 ml of TEA, the Zn vacancies are dominant, as shown by the TEM images. However, for ZnSe nanoparticles obtained by using 50 ml TEA, there are lots of stacking faults, twinning defects and some point defects as

shown in Fig. 3. Thus, the intensity of the defect-related emission of ZnSe nanoparticles obtained by using different volumes of TEA varies due to the different types of defects which are dominant in the ZnSe nanoparticles. The presence of low energy luminescence bands (the defect-related emission band) in "unintentionally" doped ZnSe provides evidence that stacking faults play a significant role in the emission. Consequently, ZnSe nanoparticles obtained by using 40 ml of TEA with a higher concentration of Zn vacancies show a higher defect-related emission, centered at 545 nm. However, ZnSe nanoparticles obtained by using 50 ml of TEA with a higher concentration of stacking faults have a stronger deep-defect emission band centered at 668 nm.

Raman spectroscopy, which has been recognized as an important structural probe, provides a fast convenient method for study of vibrational and structural properties of nano-sized materials. Many factors can influence the vibrational properties [46]. Disorder, size and shape distribution all affect the phonon spectrum. Figure 7 shows a typical room-temperature Raman spectrum of ZnSe nanoparticles obtained by using different volumes of TEA. This indicates the presence of transverse optical (TO) and longitudinal optical (LO) phonon modes. ZnSe nanoparticles obtained by using 40 ml of TEA show two Raman peaks centered at 206 and 253 $cm^{-1}$, as shown in Fig. 7a. These are attributed to the TO and LO phonon modes of ZnSe, respectively. In Fig. 7b, the obtained dominant Raman bands at 206 and 252 $cm^{-1}$ are attributed to the TO and LO phonon modes of ZnSe nanoparticles obtained by using 50 ml of TEA, respectively. No vibration modes due to impurities are observed.

From previous reports, the LO phonon frequency of single crystalline ZnSe films was 254 $cm^{-1}$ and that of single crystal ZnSe was 255 $cm^{-1}$ at room temperature and

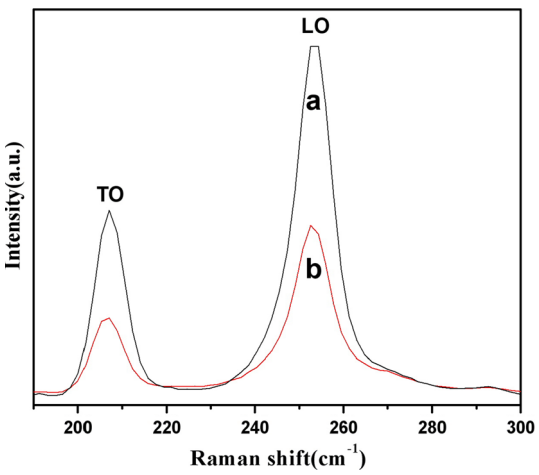


**Fig. 7** Raman spectrum of ZnSe nanoparticles synthesized using TEA, *a* 40 ml and *b* 50 ml, 514.5 nm excitation

for ZnSe polycrystalline nanoparticles, the TO and LO phonon frequencies were observed at 210 and 255 $cm^{-1}$ respectively, and gave a broad Raman peak due to the high surface to volume ratio of small particles [47]. In comparison of this result, the LO and TO phonon peaks of the synthesized ZnSe nanoparticles using different volumes of TEA are shifted towards the lower frequency, which may be due to the effect of small size and high surface area of the synthesized nanoparticles [48]. The spectral position of Raman modes has been shown to be sensitive to strain. Consequently, changes in the peak position can be used to measure residual stress [49]. For ZnSe, there are relatively few reports on the relationship between stress and the spectral position of the Raman peaks. Lin et al. [50] reported that the position of the LO mode, $\omega_{LO}$, was related to the applied hydrostatic pressure, $p$, by the relation: $\omega_{LO} = 251.9 + 3.44p - 0.02p^2$. This implies a LO peak position of 251.9 $cm^{-1}$ for stress free ZnSe, which is on the lower side of the theoretically predicted range values (252–253 $cm^{-1}$ [51]). This is in consistent with our results.

The LO and TO Raman band line widths are known to be very sensitive to the crystalline order of the material. In nanocrystals, finite-size effects have to be taken into account, and it is assumed that disorder and boundary scattering in finite-size crystals lead to a broadening of the phonon lines. The full width at half-maximum (FWHM) of the first-order LO band of our samples are 7.8 and 8.0 $cm^{-1}$ at room temperature for the sample obtained by using 40 and 50 ml of TEA. These are corrected for the instrument resolution. The TO and LO phonon modes of ZnSe nanoparticles obtained by using 50 ml TEA are a little broader than their counterparts of ZnSe nanoparticles obtained by using 40 ml of TEA. The broadening of the TO and LO phonon modes may be due to the crystalline quality and the defects in the nanoparticles obtained by using different volumes of TEA. The crystalline quality can be inferred from the peak width of the LO mode. The introduction of defects into the crystal structure leads to a decrease in phonon lifetime and a subsequent broadening of the Raman mode [52]. Thus, we consider that the broadening of the LO-phonon peak of ZnSe nanoparticles, obtained by using 50 ml compared to 40 ml of TEA, is due to the decrease in LO-phonon lifetime, as a result of disorder, defects and boundary scattering. These results are in agreement with the results of TEM.

## 4 Conclusions

In conclusion, the present TEA-assisted hydrothermal process offered a facile method to synthesize ZnSe nanoparticles with cubic zinc blende structure. TEM images showed that the average size of the synthesized ZnSe

nanoparticles decreases from 20 to 10 nm when the amount of TEA increased from 40 to 50 ml. A calibrated quantity of TEA was vital for the formation of ZnSe nanoparticles with different particle size. The PL spectra exhibited an NBE emission peak centered at 448 nm and a much wider and stronger defect-related emission band centered at 545 nm, when 40 ml of TEA was introduced into the reaction system. However, the PL spectra exhibited no NBE emission peaks, and two defect-related emission bands, one centered at 545 nm, and the other centered at 668 nm were observed when the TEA quantity increased to 50 ml. The Raman analysis results showed that the TO and LO phonon peaks in the ZnSe nanoparticles shifted towards lower wavelengths, and the LO-phonon peak of ZnSe nanoparticles obtained by using 50 ml of TEA were broader than the counterpart of ZnSe nanoparticles obtained by using 40 ml of TEA. This TEA-assisted hydrothermal method can be expanded to produce other semiconductors with controlled morphologies and size for various potential applications.

**Acknowledgments** This work was financially supported by the National Programs for High Technology Research and Development of China (863) (Item No. 2013AA032202), the National Natural Science Foundation of China (Grant Nos. 61008051, 61178074, 11204104, 11254001, 61378085, 61308095).

## References

1. D. Zhu, X. Jiang, C. Zhao, X. Sun, J. Zhang, J. Zhu, Chem. Commun. **46**, 5226–5228 (2010)
2. Y. Ni, X. Cao, G. Hu, Z. Yang, X. Wei, Y. Chen, J. Xu, Cryst. Growth Des. **7**, 280–285 (2007)
3. H. Jiang, X. Yao, J. Che, M. Wang, Mater. Res. Bull. **41**, 2349–2356 (2006)
4. Z. Deng, F.L. Lie, S. Shen, I. Ghosh, M. Mansuripur, A.J. Muscat, Langmuir **25**, 434–442 (2009)
5. P. Chen, T.Y. Xiao, H.H. Li, J.J. Yang, Z. Wang, H.B. Yao, S.H. Yu, ACS Nano. **6**, 712–719 (2012)
6. R. Xie, Y. Li, L. Jiang, X. Zhang, J. Alloys. Compd. **613**, 213–218 (2014)
7. B. Goswami, S. Pal, P. Sarkar, J. Phys. Chem. C. **112**, 11630–11636 (2008)
8. L. Yang, L. Liu, D. Xiao, J. Zhu, Mater. Lett. **72**, 113–115 (2012)
9. Y.K. Mishra, V.S.K. Chakravadhanula, V. Hrkac, S. Jebril, D.C. Agarwal, S. Mohapatra, D.K. Avasthi, L. Kienle, R. Adelung, J. Appl. Phys. **112**, 064308–064312 (2012)
10. Y.K. Mishra, S. Kaps, A. Schuchardt, I. Paulowicz, X. Jin, D. Gedamu, S. Wille, O. Lupan, R. Adelung, KONA Powder Part. J. **31**, 92–110 (2014)
11. X. Jin, M. Götz, S. Wille, Y.K. Mishra, R. Adelung, C. Zollfrank, Adv .Mater. **25**, 1342–1347 (2013)
12. V. Hrkac, L. Kienle, S. Kaps, A. Lotnyk, Y.K. Mishra, U. Schürmann, V. Duppel, B.V. Lotsch, R. Adelung, J. Appl. Crystallogr. **46**, 396–403 (2013)
13. T. Reimer, I. Paulowicz, R. Röder, S. Kaps, O. Lupan, S. Chemnitz, W. Benecke, C. Ronning, R. Adelung, Y.K. Mishra, ACS Appl. Mater. Interfaces **6**, 7806–7815 (2014)
14. Y.K. Mishra, S. Kaps, A. Schuchardt, I. Paulowicz, X. Jin, D. Gedamu, S. Freitag, M. Claus, S. Wille, A. Kovalev, S.N. Gorb, R. Adelung, Part. Part. Syst. Charact .**30**, 775–783 (2013)
15. D. Gedamu, I. Paulowicz, S. Kaps, O. Lupan, S. Wille, G. Haidarschin, Y.K. Mishra, R. Adelung, Adv. Mater. **26**, 1541–1550 (2014)
16. K. Saikia, P. Deb, E. Kalita, Curr. Appl. Phys .**13**, 925–930 (2013)
17. B.T. Huy, M.H. Seo, P.T. Phong, J.M. Lim, Y.-Ill Lee, Chem. Eng. J. **236**, 75–81 (2014)
18. Z. Chen, D. Wu, J. Lumin. **132**, 2968–2974 (2012)
19. A.L. Weaver, D.R. Gamelin, J. Am. Chem. Soc .**134**, 6819–6825 (2012)
20. J. Archana, M. Navaneethan, Y. Hayakawa, S. Ponnusamy, C. Muthamizhchelvan, Mater. Res. Bull. **47**, 1892–1897 (2012)
21. C. Ye, X. Fang, Y. Wang, P. Yan, J. Zhao, L. Zhang, Appl. Phys. A .**79**, 113–115 (2004)
22. L. Yang, R. Xie, L. Liu, D. Xiao, J. Zhu, J. Phys. Chem. C .**115**, 19507–19512 (2011)
23. B. Pejova, J. Solid State Chem. **181**, 1961–1969 (2008)
24. D. Wu, Z. Chen, G. Huang, X. Liu, Sens. Actuators A .**205**, 72–78 (2014)
25. P. Mushonga, I.L.A. Ouma, A.M. Madiehe, M. Meyer, F.B. Dejene, M.O. Onani, Phys. B. **439**, 189–192 (2014)
26. P. Kumar, J. Singh, M.K. Pandey, C.E. Jeyanthi, R. Siddheswaran, M. Paulraj, K.N. Hui, K.S. Hui, Mater. Res. Bull. **49**, 144–150 (2014)
27. F.T. Quinlan, J. Kuther, W. Tremel, W. Knoll, S. Risbud, P. Stroeve, Langmuir **16**, 4049–4051 (2000)
28. J. Zhu, Y. Koltypin, A. Gedanken, Chem. Mater. **12**, 73–78 (2000)
29. H. Zhong, Z. Wei, M. Ye, Y. Yan, Y. Zhou, Y. Ding, C. Yang, Y. Li, Langmuir **23**, 9008–9013 (2007)
30. S. Xiong, S. Huang, A. Tang, F. Teng, Mater. Lett .**61**, 5091–5094 (2007)
31. Y. Xu, N. Al-Salim, J.M. Hodgkiss, R.D. Tilley, Cryst. Growth Des. **11**, 2721–2723 (2011)
32. Y.P. Leung, Z. Liu, S.K. Hark, J. Cryst. Growth **279**, 248–257 (2005)
33. X. Wang, J. Zhu, Y. Zhang, J. Jiang, S. Wei, Appl. Phys. A .**99**, 651–656 (2010)
34. P. Reiss, New J. Chem. **31**, 1843–1852 (2007)
35. P.D. Cozzoli, L. Manna, M.L. Curri, S. Kudera, C. Giannini, M. Striccoli, A. Agostiano, Chem. Mater. **17**, 1296–1306 (2005)
36. Y. Zeng, T. Zhang, W. Fu, Q. Yu, G. Wang, Y. Zhang, Y. Sui, L. Wang, C. Shao, Y. Liu, H. Yang, G. Zou, J. Phys. Chem. C .**113**, 8016–8022 (2009)
37. R. Lv, C. Cao, H. Zhai, D. Wang, S. Liu, H. Zhu, Solid State Commun. **130**, 241–245 (2004)
38. Y. Jiang, X.M. Meng, W.C. Yiu, J. Liu, J.X. Ding, C.S. Lee, S.T. Lee, J. Phys. Chem. B. **108**, 2784–2787 (2004)
39. B.Y. Geng, Q.B. Du, X.W. Liu, J.Z. Ma, X.W. Wei, Appl. Phys. Lett. **89**, 033115–033118 (2006)
40. A.B. Panda, S. Acharya, S. Efrima, Adv. Mater. **17**, 2471–2474 (2005)
41. J. Wei, K. Li, J. Chen, J. Zhang, R. Wu, J. Alloys. Compd .**531**, 86–90 (2012)
42. S.V. Pol, V.G. Pol, J.M. Calderon-Moreno, S. Cheylan, A. Gedanken, Langmuir **24**, 10462–10466 (2008)
43. S. Xiong, J. Shen, Q. Xie, Y. Gao, Q. Tang, Y. Qian, Adv. Funct. Mater. **15**, 1787–1792 (2005)
44. X. Zhang, Z. Liu, Q. Li, Y. Leung, K. Ip, S. Hark, Adv. Mater.**17**, 1405–1410 (2005)
45. B. Xiang, H.Z. Zhang, G.H. Li, F.H. Yang, F.H. Su, R.M. Wang, J. Xu, G.W. Lu, X.C. Sun, Q. Zhao, D.P. Yu, Appl. Phys. Lett. **82**, 3330–3332 (2003)

46. P. Kumar, K. Singh, J. Lumin. **130**, 2026–2031 (2010)
47. D. Sarigiannis, J.D. Pack, G. Kioseoglou, A. Petrou, T.J. Mountziaris, Appl. Phys. Lett. **80**, 4024–4026 (2002)
48. M. Shakir, S.K. Kushwah, K.K. Maurya, G. Bhagavannarayana, M.A. Wahab, Solid State Commun. **149**, 2047–2049 (2009)
49. J.W. Ager III, M.D. Drory, Phys. Rev. B .**48**, 2601–2607 (1993)
50. C.M. Lin, D.S. Chou, T.J. Yang, W.C. Chou, J.A. Xu, E. Huang, Phys. Rev. B. **55**, 13641–13646 (1997)
51. R.K. Ram, S.S. Kushwaha, A. Shukla, Phys. Status Solidi B. **154**, 553–617 (1989)
52. C.D.O. Pickard, T.J. Davis, W.N. Wang, J.W. Steeds, Diam. Relat. Mater. **7**, 238–280 (1998)